

Standardized Data Acquisition for Neuromelanin-sensitive Magnetic Resonance Imaging of the Substantia Nigra

Garrett Salzman¹, Jocelyn Kim¹, Guillermo Horga^{*,1,2}, Kenneth Wengler^{*,1,2}

¹ New York State Psychiatric Institute ² Department of Psychiatry, Columbia University

* These authors contributed equally

Corresponding Authors

Guillermo Horga

HorgaG@nyspi.columbia.edu

Kenneth Wengler

Kenneth.Wengler@nyspi.columbia.edu

Citation

Salzman, G., Kim, J., Horga, G., Wengler, K. Standardized Data Acquisition for Neuromelanin-sensitive Magnetic Resonance Imaging of the Substantia Nigra. *J. Vis. Exp.* (175), e62493, doi:10.3791/62493 (2021).

Date Published

September 8, 2021

DOI

10.3791/62493

URL

jove.com/video/62493

Introduction

Neuromelanin (NM) is a dark pigment found in dopaminergic neurons of the substantia nigra (SN) and noradrenergic neurons of the locus coeruleus (LC)^{1,2}. NM is synthesized by the iron-dependent oxidation of cytosolic dopamine and norepinephrine and is stored in autophagic vacuoles in the

soma³. It first appears in humans around 2-3 years of age and accumulates with age^{1,4,5}.

Within the NM-containing vacuoles of SN and LC neurons, NM forms complexes with iron. These NM-iron complexes are paramagnetic, allowing for noninvasive visualization of NM using magnetic resonance imaging (MRI)^{6,7}. MRI scans that can visualize NM are known as NM-sensitive MRI

Abstract

The dopaminergic system plays a crucial role in healthy cognition (e.g., reward learning and uncertainty) and neuropsychiatric disorders (e.g., Parkinson's disease and schizophrenia). Neuromelanin is a byproduct of dopamine synthesis that accumulates in dopaminergic neurons of the substantia nigra. Neuromelanin-sensitive magnetic resonance imaging (NM-MRI) is a noninvasive method for measuring neuromelanin in those dopaminergic neurons, providing a direct measure of dopaminergic cell loss in the substantia nigra and a proxy measure of dopamine function. Although NM-MRI has been shown to be useful for studying various neuropsychiatric disorders, it is challenged by a limited field-of-view in the inferior-superior direction resulting in the potential loss of data from the accidental exclusion of part of the substantia nigra. In addition, the field is lacking a standardized protocol for the acquisition of NM-MRI data, a critical step in facilitating large-scale multisite studies and translation into the clinic. This protocol describes a step-by-step NM-MRI volume placement procedure and online quality control checks to ensure the acquisition of good-quality data covering the entire substantia nigra.

(NM-MRI) and use either direct or indirect magnetization transfer effects to provide contrast between regions with high NM concentration (e.g., the SN) and the surrounding white matter^{8,9}.

Magnetization transfer contrast is the result of the interaction between macromolecular-bound water protons (which are saturated by the magnetization transfer pulses) and the surrounding free water protons. In NM-MRI, it is believed that the paramagnetic nature of NM-iron complexes shortens the T₁ of the surrounding free water protons, resulting in reduced magnetization-transfer effects so that regions with higher NM concentration appear hyperintense on NM-MRI scans¹⁰. Conversely, the white matter surrounding the SN has a high macromolecular content, resulting in large magnetization-transfer effects so that these regions appear hypointense on NM-MRI scans, thus providing high contrast between the SN and surrounding white matter.

In the SN, NM-MRI can provide a marker of dopaminergic cell loss¹¹ and dopamine system function¹². These two processes are relevant for several neuropsychiatric disorders and are supported by a vast body of clinical and preclinical work. For example, abnormalities in dopamine function have been widely observed in schizophrenia; *in vivo* studies using positron emission tomography (PET) have shown increased striatal dopamine release^{13,14,15,16} and increased dopamine synthesis capacity^{17,18,19,20,21,22}. Furthermore, post-mortem studies have shown that patients with schizophrenia have increased levels of tyrosine hydroxylase—the rate-limiting enzyme involved in dopamine synthesis—in the basal ganglia²³ and SN^{24,25}.

Several studies have investigated patterns of dopaminergic cell loss, particularly in Parkinson's disease. Post-mortem studies have revealed that the pigmented dopaminergic

neurons of the SN are the primary site of neurodegeneration in Parkinson's disease^{26,27}, and that, while SN cell loss in Parkinson's disease is not correlated with cell loss in normal aging²⁸, it is correlated with the duration of the disease²⁹. Unlike most methods for investigating the dopaminergic system, the non-invasiveness, cost-effectiveness, and lack of ionizing radiation make NM-MRI a versatile biomarker³⁰.

The NM-MRI protocol described in this paper was developed to increase both within-subject and across-subject reproducibility of NM-MRI. This protocol ensures full coverage of the SN despite the limited coverage of NM-MRI scans in the inferior-superior direction. The protocol makes use of sagittal, coronal, and axial three-dimensional (3D) T1-weighted (T1w) images, and the steps should be followed to achieve proper slice stack placement. The protocol outlined in this paper has been utilized in multiple studies^{31,32} and was extensively tested. Wengler et al. completed a study of the reliability of this protocol in which NM-MRI images were acquired twice in each participant across multiple days³². Intra-class correlation coefficients demonstrated excellent test-retest reliability of this method for region of interest (ROI)-based and voxelwise analyses, as well as high contrast in the images.

Protocol

NOTE: The research conducted to develop this protocol was performed in compliance with New York State Psychiatric Institute Institutional Review Board guidelines (IRB #7655). One subject was scanned for recording the protocol video, and written informed consent was obtained. Refer to the **Table of Materials** for details about the MRI scanner used in this protocol.

1. MRI acquisition parameters

1. Prepare to acquire high-resolution T1w images using a 3D magnetization prepared rapid acquisition gradient echo (MPRAGE) sequence with the following parameters: spatial resolution = $0.8 \times 0.8 \times 0.8 \text{ mm}^3$; field-of-view (FOV) = $176 \times 240 \times 240 \text{ mm}^3$; echo time (TE) = 3.43 ms; repetition time (TR) = 2462 ms; inversion time (TI) = 1060 ms; flip angle = 8° ; in-plane parallel imaging factor (ARC) = 2; through-plane parallel imaging factor (ARC) = 2^{33} ; bandwidth = 208 Hz/pixel; total acquisition time = 6 min 39 s.
2. Prepare to acquire NM-MRI images using a two-dimensional (2D) gradient recalled echo sequence with magnetization transfer contrast (2D GRE-MTC) with the following parameters: resolution = $0.43 \times 0.43 \text{ mm}^2$; FOV = $220 \times 220 \text{ mm}^2$; slice-thickness = 1.5 mm; 20 slices; slice gap = 0 mm; TE = 4.8 ms; TR = 500 ms; flip angle = 40° ; bandwidth = 122 Hz/pixel; MT frequency offset = 1.2 kHz; MT pulse duration = 8 ms; MT flip angle = 670° ; number of averages = 5; total acquisition time = 10 min 4 s.

NOTE: Although the displayed results used these MRI acquisition parameters, this protocol is valid for various T1w and NM-MRI imaging protocols. The NM-MRI protocol should cover ~25 mm in the inferior-superior direction to guarantee complete coverage of the SN.

2. Placement of NM-MRI volume

1. Acquire a high-resolution T1w image ($\leq 1 \text{ mm}$ isotropic voxel size). Use online reformatting directly after image acquisition to create high-resolution T1w images aligned

to the anterior commissure-posterior commissure (AC-PC) line and the midline.

1. Carry out online reformatting using the vendor-provided software (e.g., if acquiring data on a GE scanner: MultiPlanar Reconstruction (MPR) in **Planning**; if acquiring data on a Siemens scanner: MPR in the **3D Task Card**; if acquiring data on a Philips scanner: MPR in the **Render Mode** of the **VolumeView Package**).
 1. Create multiplanar reconstructions of the 3D T1w image in the axial plane perpendicular to the AC-PC line to cover the whole brain with minimal slice-gap.
 2. Create multiplanar reconstructions of the 3D T1w image in the coronal plane perpendicular to the AC-PC line to cover the whole brain with minimal slice-gap.
 3. Create multiplanar reconstructions of the 3D T1w image in the sagittal plane parallel to the AC-PC line to cover the whole brain with minimal slice-gap.
2. Load the sagittal, coronal, and axial views of the reformatted high-resolution T1w image and ensure that reference lines depicting the location of each displayed slice are present.
3. Identify the sagittal image that shows the largest separation between the midbrain and thalamus (**Figure 1A**). To do this, visually inspect the sagittal slices of the reformatted T1w image until the slice showing this greatest separation is identified.
4. Using the sagittal image from the end of step 2.3, visually identify the coronal plane that delineates the most anterior aspect of the midbrain (**Figure 1B**).

5. Using the coronal image from the end of step 2.4, visually identify the axial plane that delineates the inferior aspect of the third ventricle (**Figure 1C**).
6. On the sagittal image from the end of step 2.3, align the superior boundary of the NM-MRI volume to the axial plane identified in step 2.5 (**Figure 1D**).
7. Move the superior boundary of the NM-MRI volume 3 mm in the superior direction (**Figure 1E**).
8. Align the NM-MRI volume to the midline in the axial and coronal images (**Figure 1F**).
9. Acquire the NM-MRI images.

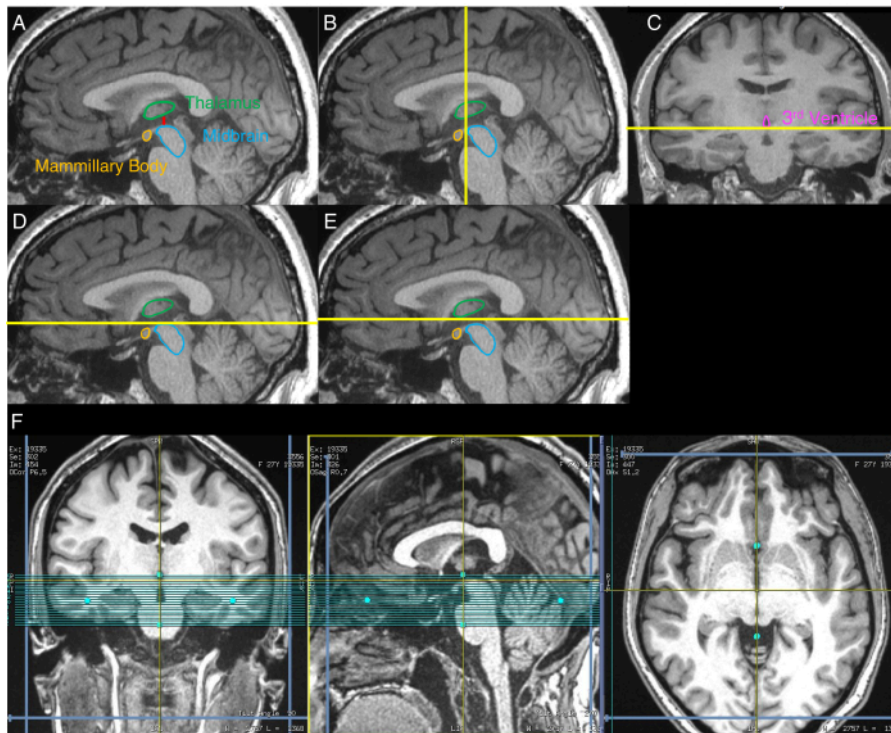


Figure 1: Images displaying the step-by-step NM-MRI volume placement procedure. Yellow lines indicate the location of the slices used for volume placement as described in the protocol. **(A)** First, the sagittal image with the greatest separation between the midbrain and thalamus is identified (step 2.3 of the protocol). **(B)** Second, using the image from **A**, the coronal plane delineating the most anterior aspect of the midbrain is identified (step 2.4). **(C)** Third, on the coronal image from the plane identified in **B**, the axial plane delineating the inferior aspect of the third ventricle is identified (step 2.5). **(D)** Fourth, the axial plane identified in **C** is displayed on the sagittal image from **A** (step 2.6). **(E)** Fifth, the axial plane from **D** is shifted 3 mm in the superior direction, and this plane indicates the superior boundary of the NM-MRI volume (step 2.7). **(F)** The final NM-MRI volume placement where the coronal image corresponds to **C**, the sagittal image corresponds to **A**, and the axial image corresponds to the axial plane in **E**. The NM-MRI volume is aligned to the brain midline in the coronal and axial images and the AC-PC line in the sagittal image (step 2.8). Part of this figure has been reprinted with permission from Elsevier from ³⁰. Abbreviations: NM-MRI = neuromelanin-sensitive magnetic resonance imaging; AC-PC = anterior commissure-posterior commissure. [Please click here to view a larger version of this figure.](#)

3. Quality control checks

1. Ensure that the acquired NM-MRI images cover the entire SN and that the SN is visible in the central

images but not in the most superior or most inferior images of the NM-MRI volume. Otherwise (**Figure 2**), repeat steps 2.3-2.9 to ensure correct NM-MRI volume placement. If the participant has moved significantly

since the acquisition of the high-resolution T1w scan, repeat steps 2.1-2.9.

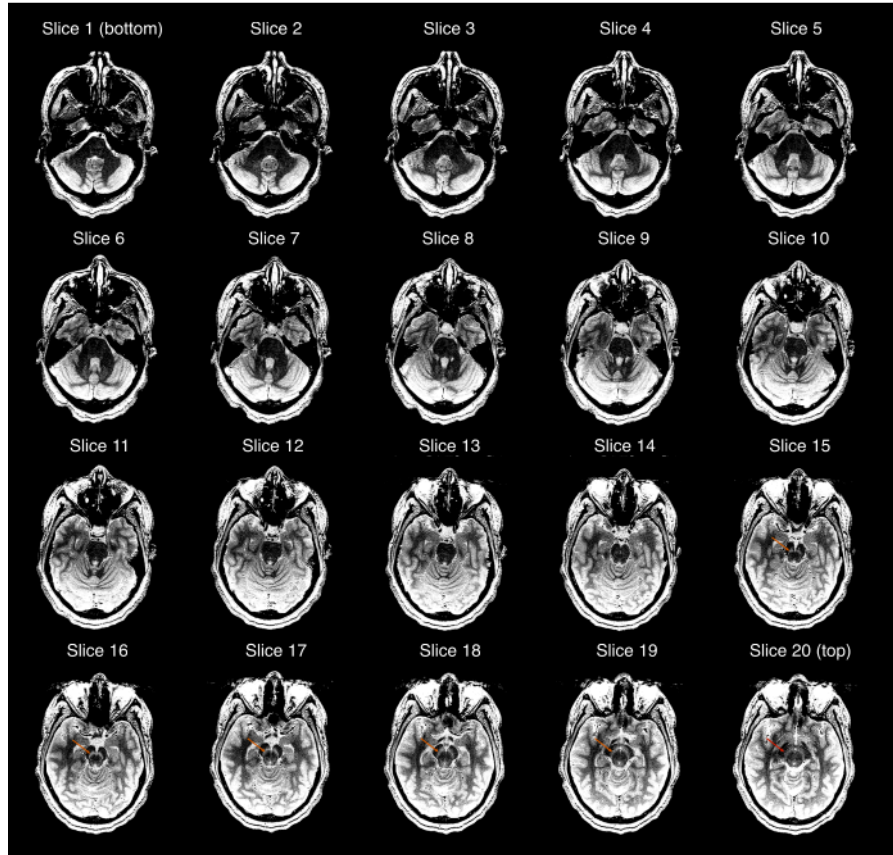


Figure 2: Example of an NM-MRI acquisition that failed the first quality control check (step 3.1 of the protocol). Each of the 20 NM-MRI slices displayed from most inferior (top left image) to most superior (bottom right image); the image window/level was set to exaggerate the contrast between the substantia nigra and crus cerebri. The orange arrows in slices 15-19 show the location of the substantia nigra in those slices. The red arrow in the most superior slice (slice 20) shows that the substantia nigra is still visible in this slice, and thus, the acquisition fails the quality check. Abbreviation: NM-MRI = neuromelanin-sensitive magnetic resonance imaging. [Please click here to view a larger version of this figure.](#)

2. Check for artifacts, particularly ones that go through the SN and the surrounding white matter, by visually inspecting each slice of the acquired NM-MRI scan.
 1. Look for abrupt changes in signal intensity with a linear pattern that does not respect normal

anatomical boundaries. For example, this may appear as a low-intensity region that is flanked by two high-intensity regions.

2. If the artifact is the result of blood vessels (**Figure 3A**), retain the NM-MRI images because these artifacts will most likely always be present.

3. If the artifacts are the result of participant head motion (**Figure 3B**), remind the participant to stay as still as possible and reacquire the NM-MRI images according to step 3.2.5.
4. If the artifacts are ambiguous (**Figure 3C**), reacquire the NM-MRI images according to step 3.2.5. Upon reacquisition, if the artifacts remain present, proceed with these images as they are likely biological rather than a result of acquisition issues.
5. If the NM-MRI images pass the quality control check in step 3.1, copy the previous NM-MRI volume placement. If the NM-MRI images fail the quality control check in step 3.1, repeat steps 2.3-2.9 to ensure correct NM-MRI volume placement (or steps 2.1-2.9 if the participant moved significantly).

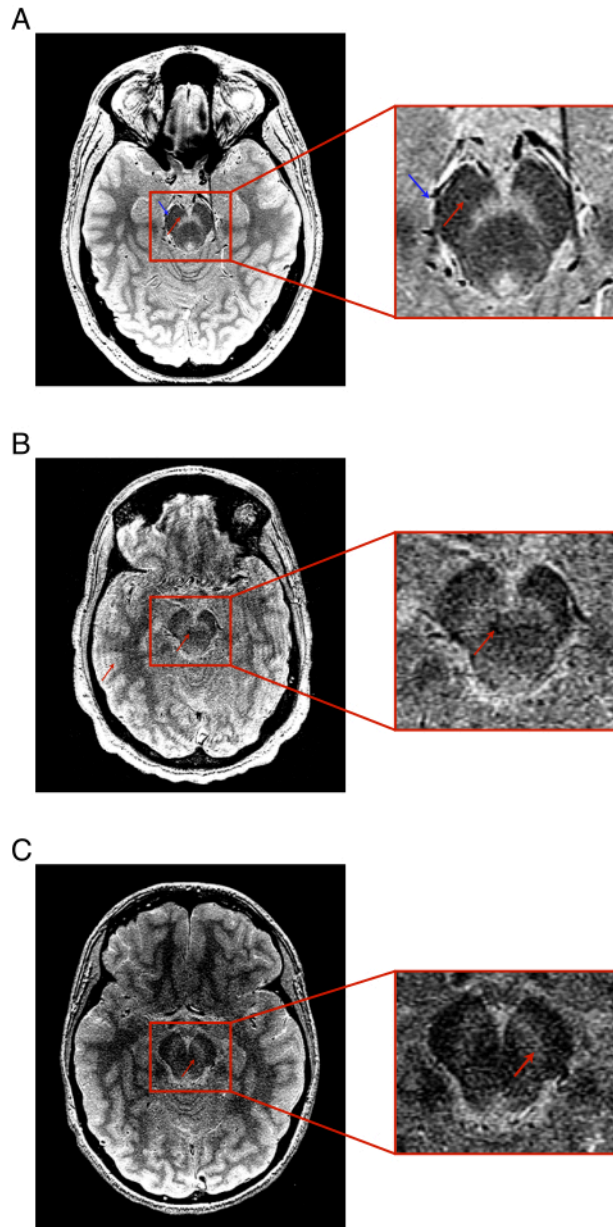


Figure 3: Examples of NM-MRI acquisitions that failed the second quality control check (step 3.2 of the protocol). Only one representative slice is shown for each case. **(A)** An NM-MRI acquisition that fails the quality control check due to a blood vessel artifact (red arrows) that is the result of the blood vessel identified by the blue arrows. **(B)** An NM-MRI acquisition that fails the quality control check due to motion artifacts (red arrows). **(C)** An NM-MRI acquisition that fails the quality control check due to an ambiguous artifact (red arrows). Abbreviation: NM-MRI = neuromelanin-sensitive magnetic resonance imaging. [Please click here to view a larger version of this figure.](#)

Representative Results

Figure 4 shows the representative results from a 28-year-old female participant with no psychiatric or neurological disorders. The NM-MRI protocol ensures complete coverage of the SN, achieved by following step 2 of the protocol outlined in **Figure 1**, and satisfactory NM-MRI images by following step 3 of the protocol. Excellent contrast between the SN

and neighboring white matter regions with negligible NM concentration (i.e., crus cerebri) can be seen. These images were checked immediately after acquisition to ensure the proper coverage of the SN and to check for artifacts. Because full coverage of the SN was achieved without any artifacts, the scan passed the quality checks and did not need to be repeated.

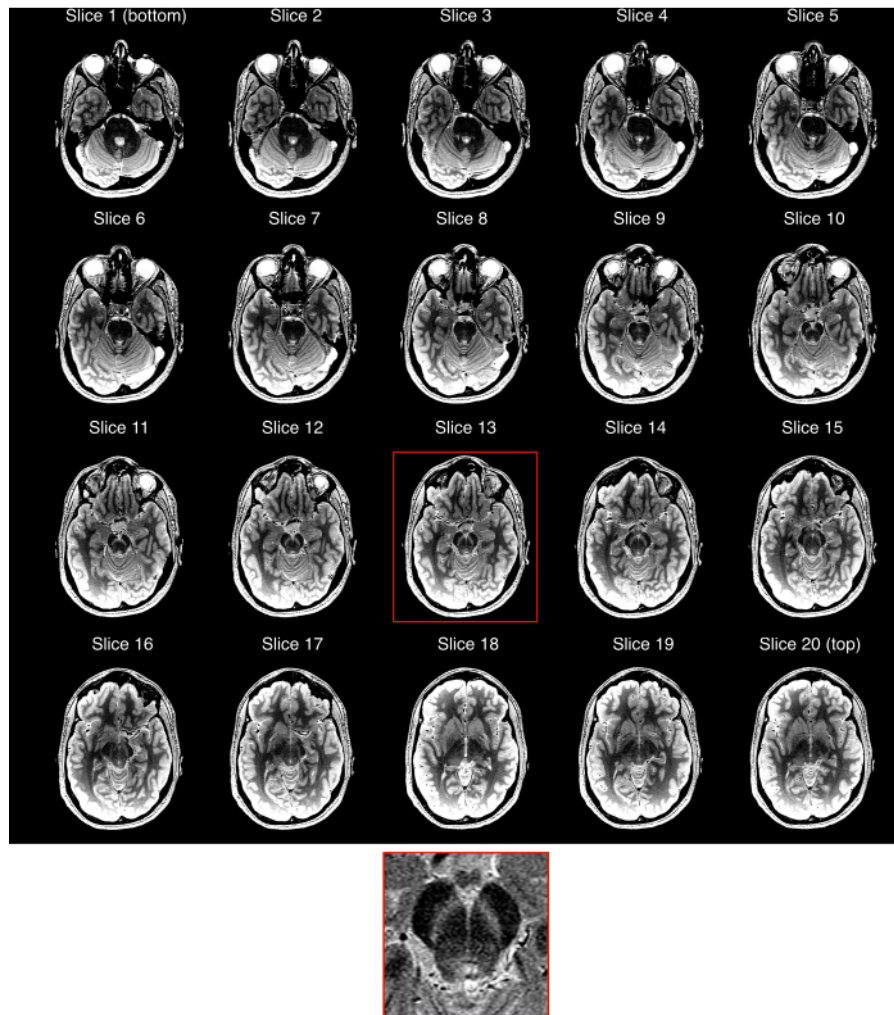


Figure 4: Example of a representative NM-MRI acquisition. Each of the 20 NM-MRI slices displayed from most inferior (top left image) to most superior (bottom right image); the image window/level was set to exaggerate the contrast between the substantia nigra and crus cerebri from a 28-year-old female participant with no psychiatric or neurological disorders. The NM-MRI protocol ensures complete coverage of the substantia nigra, partial coverage of the locus coeruleus, and satisfactory NM-MRI images. Excellent contrast between the substantia nigra and neighboring white matter regions with no neuromelanin concentration (i.e., crus cerebri) can be seen on slices 9-16. The image at the bottom shows a zoomed-in view of the midbrain from slice 13. Abbreviation: NM-MRI = neuromelanin-sensitive magnetic resonance imaging. [Please click here to view a larger version of this figure.](#)

Figure 2 shows the representative results from a 28-year-old female participant with no psychiatric or neurological disorders whose images failed the first quality control check

(step 3.1). The SN is visible in the most superior slice (slice 20), indicating that full coverage of the SN was not achieved. In this instance, the data must be reacquired by repeating

steps 2.3-2.9 of the protocol, as shown in **Figure 1**. If the participant has moved significantly since the acquisition of the initial T1w image, then the researcher should return to step 2.1 to reacquire the T1w image.

Figure 3 shows example images that failed the second quality control check (step 3.2). As outlined in step 3.2, scans containing artifacts due to blood vessels (**Figure 3A**) do not need to be repeated, as those artifacts will likely be present in every acquisition. Scans that contain artifacts resulting from motion (**Figure 3B**) or ambiguous artifacts (**Figure 3C**) should be repeated. In the case of ambiguous artifacts, if the artifacts remain present after reacquisition, then the scan does not need to be reacquired further as the artifacts are likely biological and therefore, will be present in every acquisition.

Discussion

The dopaminergic system plays a crucial role in healthy cognition and neuropsychiatric disorders. The development of noninvasive methods that can be used to repeatedly investigate the dopaminergic system *in vivo* is critical for the development of clinically meaningful biomarkers. The protocol described here supplies step-by-step instructions for acquiring good-quality NM-MRI images of the SN, including placement of the NM-MRI volume and quality control checks to ensure usable data.

Even though detailed protocols for analysis of NM-MRI data have been discussed elsewhere, for completeness, we provide a brief summary of our previous work and recommendations for preprocessing of NM-MRI images and voxelwise analyses. This approach has been validated previously in conjunction with the acquisition protocol described in this paper. Previous studies discuss the advantages of this method in more detail and provide

data supporting its reproducibility^{6,12,32}. Note however that the standardized acquisition protocol described herein is applicable to any processing and analysis strategy (including ROI-based analysis in native or MNI space^{8,32}) and not just the one described here.

For analysis of NM-MRI images, preprocessing can be performed to correct for motion and to spatially normalize individual subject data to a standard anatomical template. We recommend the following pipeline combining Statistical Parametric Mapping (SPM) and Advanced Normalization Tools (ANTs) to use the following tools in the following steps: (1) **SPM-Realign** to realign and correct separately acquired averages for motion, and **SPM-ImCalc** to average the realigned images; (2) **antsBrainExtraction.sh** for brain extraction of the T1w image; (3) **antsRegistrationSyN.sh** (rigid + affine + deformable syn) for spatial normalization of the brain-extracted T1w image to the MNI152NLin2009cAsym template space; (4) **antsRegistrationSyN.sh** (rigid) to coregister the NM-MRI image to the T1w (in native space) image; (5) **antsApplyTransforms** to combine the transformations estimated in steps 3 and 4 into a single-step transformation for spatial normalization of the NM-MRI images to MNI space; and (6) **SPM-Smooth** with a 1 mm full-width-at-half-maximum Gaussian kernel for spatial smoothing of the spatially normalized NM-MRI image. This processing pipeline was previously shown to achieve the highest test-retest reliability in the literature, with an average intra-class correlation coefficient (ICC) within the SN of ~ 0.90 ³². Furthermore, several previous studies have used similar preprocessing pipelines^{12,31,34,35,36,37}.

After spatial normalization, the NM-MRI images should be analyzed by calculating the contrast-to-noise ratio at each

voxel (CNR_V). The CNR measures the percent signal difference between each voxel (I_V) and a reference white matter region known to have little NM content¹² (crus cerebri, I_{CC}), given by the following formula: $CNR_V = \{[I_V - \text{mode}(I_{CC})] / \text{mode}(I_{CC})\} * 100$. CNR_V values can be averaged for each participant to determine the CNR of the entire SN or can be analyzed at the voxelwise level within the SN. Higher CNR values reflect increased NM content in that voxel or ROI. Unlike some other analysis methods that define the SN ROI as the hyperintense region in a NM-MRI image, this recommended method uses predefined template ROIs that can be obtained from the literature¹² or drawn on the average of NM-MRI images in MNI space across all subjects in the study (using a study-specific template). Not only is this method fully automated, it also removes circularity in the analysis, accounts for heterogeneity within the SN-VTA complex, and does not limit analysis to the whole-ROI level.

When acquiring NM-MRI images, it is critical that the T1w images used to place the NM-MRI volume are aligned along the AC-PC line. Doing so will improve the reproducibility of the scans. It is also important to acquire the T1w images as close in time before acquiring the NM-MRI images as possible. Because the T1w image is used for NM-MRI volume placement, it is important that it accurately represents the location of the participant's head in the scanner. If the participant has moved between the T1w scan and the NM-MRI scan, then the NM-MRI volume will not be appropriately placed. Minimizing the amount of time between acquisition of the T1w images and the NM-MRI images will decrease the likelihood that the participant has moved between scans and therefore decrease the likelihood that part of the SN is not included in the NM-MRI volume.

Some modifications to the protocol may be required if issues with the NM-MRI acquisition arise. If the whole SN is not consistently covered, even after correcting the volume placement, then the number of slices in the NM-MRI protocol may need to be increased to capture the entire SN. Additionally, if the participant has difficulty staying still for the entirety of the NM-MRI scan, resulting in consistent motion artifacts, individual repetitions could be acquired and averaged offline. For example, instead of completing one 10-min scan that acquires five repetitions averaged online, five 2-min scans could be acquired and averaged offline. This would give the participant opportunities for breaks in between repetitions and may help them remain still for the duration of the individual scans.

One limitation of this protocol is that it does not provide full coverage of the LC with standard NM-MRI acquisition protocols, preventing the noradrenergic system from being thoroughly investigated using this method. While the LC is a structure that can be imaged using NM-MRI, including the LC in this protocol would increase the number of slices required to reliably capture both the SN and LC in their entirety. Increasing the number of slices would, in turn, increase the scan time for this protocol. Because these scans are sensitive to motion, an increase in scan time may produce lower-quality images as participants may find it more difficult to remain still for longer periods—particularly problematic in clinical populations. Thus, we chose not to include the LC in this protocol to minimize the potential for motion artifacts in the data. Future studies should investigate the reliability of NM-MRI protocols with a greater number of slices to simultaneously image the SN and LC.

A second limitation of this protocol is that the AC-PC alignment of the NM-MRI volume may not provide the optimal

orientation for imaging the SN. While the AC-PC line is easy to identify, this orientation does not fully minimize partial volume effects as it is not perfectly perpendicular to the SN. Previous work has utilized an oblique axial section perpendicular to the floor of the fourth ventricle to image the SN^{38,39,40}. While this volume placement, or one perpendicular to the cerebral aqueduct, may provide less partial volume effects than AC-PC alignment, we chose to use the AC-PC line given its clearly defined landmarks. The validity of this alignment was shown in previous work utilizing the protocol outlined above, in which excellent test-retest reliability was achieved³². AC-PC alignment has also been used in several other studies. Cassidy et al. found that patients with cocaine addiction had higher SN CNR values than controls³⁵. In a study of patients with late-life depression, Wengler et al. found that psychomotor function was correlated with SN CNR values³⁶. A third paper also found that Parkinson's patients had reduced CNR in the SN while patients with psychosis had increased CNR in the SN¹².

However, no study has directly compared different volume placement methods, and this is an area that future research should explore to determine which method provides the best test-retest reliability across multiple acquisitions. 3D NM-MRI sequences could provide an alternative solution because they provide greater flexibility in reformatting after acquisition. Furthermore, 3D sequences achieve a higher signal-to-noise ratio than 2D sequences, potentially allowing for higher spatial resolution but come at the cost of increased sensitivity to motion. Currently, 2D-GRE MT is the only extensively validated NM-MRI sequence—the motivating factor for using it for this protocol. Future studies should compare NM-MRI signal from 3D sequences to NM concentration and striatal

dopamine function, and reproducibility in comparison to 2D-GRE MT before widespread adoption.

This protocol has advantages over other NM-MRI protocols because it provides easily identifiable landmarks for NM-MRI volume placement, making it highly reproducible. It also provides online quality checks, which no other NM-MRI protocol has included. These quality checks allow the experimenter to reacquire images if they are of poor quality rather than simply excluding that subject from the analysis.

NM-MRI is a valuable tool that has been used to investigate several neuropsychiatric disorders. NM-MRI is a proxy measure of dopamine function in the nigrostriatal pathway¹², thus offering a method of examining the *in vivo* dopaminergic system that does not require invasive procedures such as PET. Patients with schizophrenia have increased NM signal in the SN^{38,41}, supporting previous studies that have revealed increased dopaminergic function in schizophrenia. NM-MRI signal in the SN also correlates with psychosis severity in patients with schizophrenia and those at high risk for schizophrenia¹². Research has also shown that individuals with cocaine use disorder have increased NM-MRI signal in the ventrolateral regions of the SN³⁵, and that in patients with late-life depression, lower NM-MRI signal in the SN is correlated with motor slowing³⁶. Additionally, NM-MRI has been used to study dopaminergic cell loss in conditions such as Parkinson's disease.

Kitao and colleagues established that NM-MRI signal in the SN is correlated with the number of pigmented dopaminergic neurons in the SN¹¹, and others have shown that NM-MRI signal in SN dopaminergic neurons is decreased in Parkinson's disease^{6,9,39,40}. Further research in Parkinson's patients has used NM-MRI to map the topographical pattern of SN cell loss¹² and the progression

of SN cell loss over the course of the disease³⁷. Altogether, this suggests that not only does NM-MRI provide insight into the underlying chemical components of neuropsychiatric disorders, but it may also be useful as a biomarker in predicting disease onset and severity. We hope that the standardized protocol presented here will facilitate future work to develop clinically useful biomarkers based on NM-MRI³⁰.

Disclosures

None.

Acknowledgments

None.

References

1. Zecca, L. et al. New melanic pigments in the human brain that accumulate in aging and block environmental toxic metals. *Proceedings of the National Academy of Sciences of the United States of America*. **105** (45), 17567-17572 (2008).
2. Zucca, F. A. et al. The neuromelanin of human substantia nigra: physiological and pathogenic aspects. *Pigment Cell Research*. **17** (6), 610-617 (2004).
3. Sulzer, D. et al. Neuromelanin biosynthesis is driven by excess cytosolic catecholamines not accumulated by synaptic vesicles. *Proceedings of the National Academy of Sciences of the United States of America*. **97** (22), 11869-11874 (2000).
4. Cowen, D. The melanoneurons of the human cerebellum (nucleus pigmentosus cerebellaris) and homologues in the monkey. *Journal of Neuropathology & Experimental Neurology*. **45** (3), 205-221 (1986).
5. Zecca, L. et al. The absolute concentration of nigral neuromelanin, assayed by a new sensitive method, increases throughout the life and is dramatically decreased in Parkinson's disease. *FEBS Letters*. **510** (3), 216-220 (2002).
6. Sulzer, D. et al. Neuromelanin detection by magnetic resonance imaging (MRI) and its promise as a biomarker for Parkinson's disease. *NPJ Parkinson's Disease*. **4** (1), 11 (2018).
7. Zucca, F. A. et al. Neuromelanin organelles are specialized autolysosomes that accumulate undegraded proteins and lipids in aging human brain and are likely involved in Parkinson's disease. *NPJ Parkinson's Disease*. **4** (1), 17 (2018).
8. Chen, X. et al. Simultaneous imaging of locus coeruleus and substantia nigra with a quantitative neuromelanin MRI approach. *Magnetic Resonance Imaging*. **32** (10), 1301-1306 (2014).
9. Sasaki, M. et al. Neuromelanin magnetic resonance imaging of locus ceruleus and substantia nigra in Parkinson's disease. *Neuroreport*. **17** (11), 1215-1218 (2006).
10. Trujillo, P. et al. Contrast mechanisms associated with neuromelanin-MRI. *Magnetic Resonance in Medicine*. **78** (5), 1790-1800 (2017).
11. Kitao, S. et al. Correlation between pathology and neuromelanin MR imaging in Parkinson's disease and dementia with Lewy bodies. *Neuroradiology*. **55** (8), 947-953 (2013).
12. Cassidy, C. M. et al. Neuromelanin-sensitive MRI as a noninvasive proxy measure of dopamine function in the human brain. *Proceedings of the National Academy*

- of Sciences of the United States of America. **116** (11), 5108-5117 (2019).
13. Abi-Dargham, A. et al. Increased striatal dopamine transmission in schizophrenia: confirmation in a second cohort. *American Journal of Psychiatry*. **155** (6), 761-767 (1998).
 14. Laruelle, M. et al. Single photon emission computerized tomography imaging of amphetamine-induced dopamine release in drug-free schizophrenic subjects. *Proceedings of the National Academy of Sciences of the United States of America*. **93** (17), 9235-9240 (1996).
 15. Breier, A. et al. Schizophrenia is associated with elevated amphetamine-induced synaptic dopamine concentrations: evidence from a novel positron emission tomography method. *Proceedings of the National Academy of Sciences of the United States of America*. **94** (6), 2569-2574 (1997).
 16. Abi-Dargham, A. et al. Increased baseline occupancy of D-2 receptors by dopamine in schizophrenia. *Proceedings of the National Academy of Sciences of the United States of America*. **97** (14), 8104-8109 (2000).
 17. Hietala, J. et al. Presynaptic dopamine function in striatum of neuroleptic-naive schizophrenic patients. *Lancet*. **346** (8983), 1130-1131 (1995).
 18. Lindström, L. H. et al. Increased dopamine synthesis rate in medial prefrontal cortex and striatum in schizophrenia indicated by L-(β -11C) DOPA and PET. *Biological Psychiatry*. **46** (5), 681-688 (1999).
 19. Meyer-Lindenberg, A. et al. Reduced prefrontal activity predicts exaggerated striatal dopaminergic function in schizophrenia. *Nature Neuroscience*. **5** (3), 267-271 (2002).
 20. McGowan, S., Lawrence, A. D., Sales, T., Queded, D., Grasby, P. Presynaptic dopaminergic dysfunction in schizophrenia: a positron emission tomographic [18F] fluorodopa study. *Archives of General Psychiatry*. **61** (2), 134-142 (2004).
 21. Bose, S. K. et al. Classification of schizophrenic patients and healthy controls using [18F] fluorodopa PET imaging. *Schizophrenia Research*. **106** (2-3), 148-155 (2008).
 22. Kegeles, L. S. et al. Increased synaptic dopamine function in associative regions of the striatum in schizophrenia. *Archives of General Psychiatry*. **67** (3), 231-239 (2010).
 23. Toru, M. et al. Neurotransmitters, receptors and neuropeptides in post-mortem brains of chronic schizophrenic patients. *Acta Psychiatrica Scandinavica*. **78** (2), 121-137 (1988).
 24. Perez-Costas, E., Melendez-Ferro, M., Rice, M. W., Conley, R. R., Roberts, R. C. Dopamine pathology in schizophrenia: analysis of total and phosphorylated tyrosine hydroxylase in the substantia nigra. *Frontiers in Psychiatry*. **3**, 31 (2012).
 25. Howes, O. D. et al. Midbrain dopamine function in schizophrenia and depression: a post-mortem and positron emission tomographic imaging study. *Brain*. **136** (11), 3242-3251 (2013).
 26. Bernheimer, H., Birkmayer, W., Hornykiewicz, O., Jellinger, K., Seitelberger, F. Brain dopamine and the syndromes of Parkinson and Huntington Clinical, morphological and neurochemical correlations. *Journal of the Neurological Sciences*. **20** (4), 415-455 (1973).

27. Hirsch, E., Graybiel, A. M., Agid, Y. A. Melanized dopaminergic neurons are differentially susceptible to degeneration in Parkinson's disease. *Nature*. **334** (6180), 345 (1988).
28. Fearnley, J. M., Lees, A. J. Ageing and Parkinson's disease: substantia nigra regional selectivity. *Brain*. **114** (5), 2283-2301 (1991).
29. Damier, P., Hirsch, E., Agid, Y., Graybiel, A. The substantia nigra of the human brain: II. Patterns of loss of dopamine-containing neurons in Parkinson's disease. *Brain*. **122** (8), 1437-1448 (1999).
30. Horga, G., Wengler, K., Cassidy, C. M. Neuromelanin-sensitive magnetic resonance imaging as a proxy marker for catecholamine function in psychiatry. *JAMA Psychiatry*. **78** (7), 788-789 (2021).
31. Wengler, K. et al. Cross-scanner harmonization of neuromelanin-sensitive MRI for multisite studies. *Journal of Magnetic Resonance Imaging*. (2021).
32. Wengler, K., He, X., Abi-Dargham, A., Horga, G. Reproducibility assessment of neuromelanin-sensitive magnetic resonance imaging protocols for region-of-interest and voxelwise analyses. *NeuroImage*. **208**, 116457 (2020).
33. Griswold, M. A. et al. Generalized autocalibrating partially parallel acquisitions (GRAPPA). *Magnetic Resonance in Medicine*. **47** (6), 1202-1210 (2002).
34. van der Pluijm, M. et al. Reliability and reproducibility of neuromelanin-sensitive imaging of the substantia nigra: a comparison of three different sequences. *Journal of Magnetic Resonance Imaging*. **53** (5), 712-721 (2020).
35. Cassidy, C. M. et al. Evidence for dopamine abnormalities in the substantia nigra in cocaine addiction revealed by neuromelanin-sensitive MRI. *American Journal of Psychiatry*. **177** (11), 1038-1047 (2020).
36. Wengler, K. et al. Association between neuromelanin-sensitive MRI signal and psychomotor slowing in late-life depression. *Neuropsychopharmacology*. **46**, 1233-1239 (2020).
37. Biondetti, E. et al. Spatiotemporal changes in substantia nigra neuromelanin content in Parkinson's disease. *Brain*. **143** (9), 2757-2770 (2020).
38. Shibata, E. et al. Use of neuromelanin-sensitive MRI to distinguish schizophrenic and depressive patients and healthy individuals based on signal alterations in the substantia nigra and locus ceruleus. *Biological Psychiatry*. **64** (5), 401-406 (2008).
39. Fabbri, M. et al. Substantia nigra neuromelanin as an imaging biomarker of disease progression in Parkinson's disease. *Journal of Parkinson's Disease*. **7** (3), 491-501 (2017).
40. Matsuura, K. et al. Neuromelanin magnetic resonance imaging in Parkinson's disease and multiple system atrophy. *European Neurology*. **70** (1-2), 70-77 (2013).
41. Watanabe, Y. et al. Neuromelanin magnetic resonance imaging reveals increased dopaminergic neuron activity in the substantia nigra of patients with schizophrenia. *PLoS One*. **9** (8), e104619 (2014).